Enhancing TiO2 Precipitation process through the Utilization of Solution-Gas-Solid Multiphase CFD Simulation and Experiments

Junhee Han *, Minchul Ha , Junteak Lee , Donghyun Kim , Dohyung Lee *

Posted Date: 13 September 2023

doi: 10.20944/preprints202309.0877.v1

Keywords: Precipitation process; Multiphase CFD simulation; Titanium Dioxide; Particle size; Particle distribution; Thermal mixing rate

Article

Enhancing TiO_2 Precipitation Process through the Utilization of Solution-Gas-Solid Multiphase CFD Simulation and Experiments

Junhee Han [1], Minchul Ha [2], Junteak Lee [2], Donghyun Kim [2] and Dohyung Lee [3,*]

[1] Department of Mechanical engineering, Hanyang University, Seoul 04763, KOREA; wunderval@nate.com
[2] Department of Research & Development, Cosmochem.Co,.Ltd, Ulsan 45010, KOREA; mcha@cosmochem.co.kr (M.H.), jtlee@cosmochem.co.kr (J.L.), dhkim@cosmochem.co.kr (D.K.)
[3] Department of Mechanical engineering, Hanyang University, Ansan, Gyeonggi-do 15588, KOREA; dohyung@hanyang.ac.kr
* Correspondence: dohyung@hanyang.ac.kr

Abstract: The production of anatase titanium dioxide particles plays a crucial role in the sulfate process used for manufacturing white pigment. A key factor in improving the quality of white pigments is enhancing the thermal mixing process within the precipitation tank. This improvement ensures the uniform dispersion of seed particles instead of their agglomeration, leading to the formation of particles with uniform sizes. The objective of this study was to enhance three-phase CFD simulations involving the mixing process of H_2SO_4 solution, steam as a gas phase, and solid seed particles. By analyzing the trajectories of the seed particles using CFD, the optimal injection position for the seed particles within the mixing process was determined. Subsequently, lab scale test and real field test were conducted based on the insights gained from the CFD simulations. The particle size distribution of two different types of seed inlets was analyzed and compared using Transmission Electron Microscopy (TEM). The findings of this study demonstrate that the developed multi-phase CFD simulation can be effectively utilized to enhance the precipitation process for the production of anatase titanium dioxide particles.

Keywords: precipitation process; multiphase CFD simulation; titanium dioxide; particle size; particle distribution; thermal mixing rate

1. Introduction

Titanium dioxide is a widely used white pigment in industries such as coatings, paints, paper, plastic, rubber, ceramics, and textiles. There are two main structures of titanium dioxide particles: rutile and anatase, depending on the production method [1]. The sulfate process, which involves the decomposition of titanium-containing raw materials using sulfuric acid and the precipitation of titanium sulfate, will be the focus of this paper [2]. Another method is the chloride process [3]. The chemical equations for the sulfate process are shown in Eq (1).

$$FeTiO_3 + 2H_2SO_4 \rightarrow FeSO_4 + TiOSO_4 + 2H_2O$$

$$TiOSO_4 + (n+1)H_2O \rightarrow TiO_2 \bullet nH_2O + H_2SO_4 \quad (1)$$

$$TiO_2 \bullet H_20 \rightarrow TiO_2 + nH_20$$

To produce a high-quality white pigment, a stable and precise process control of precipitation is required and most $\boldsymbol{TiO_2}$ manufacturing companies have attempted to optimize the process. [4–8]. The uniformity of particle size during the precipitation process is essential for producing high-quality $\boldsymbol{TiO_2}$ pigments. If particles of varying sizes are produced, they may block the pores of the filter cloth in the following washing process [9]. Inconsistent particle sizes during precipitation can also destabilize the titanyl sulfate solution and affect the washing and preceding processes negatively. To

Preprints (www.preprints.org) | NOT PEER-REVIEWED | Posted: 13 September 2023 doi:10.20944/preprints202309.0877.v1

ensure a stable precipitation process with uniform particle size distribution, the agitator in the precipitation tank must meet two specified conditions.

Firstly, the agitator must effectively mix the solution and keep the temperature consistent during the precipitation stages. Secondly, the early injection of seed particles must be rapidly and evenly dispersed.

Many researchers in the chemical field have performed experiments to study this agglomeration [10–14]. However, studies analyzing the precipitation process using CFD are extremely limited and there is no design of precipitation through multiphase analysis [15–17]. The scarcity of information on the design parameters of agitators in chemical engineering can be attributed to the limited mechanical knowledge regarding mixing efficiency and seed diffusivity based on the shape and location of agitators. In addition, there is a need for more research data on the hydrodynamic characteristics of agitators that incorporate chemical reactions in the field of mechanical engineering.

This study aims to utilize multi-phase CFD for the first time in the precipitation process, to combine knowledge from both chemical and mechanical engineering to understand the impact of various design parameters of agitators on the particle size distribution of $\boldsymbol{TiO_2}$ pigments. Additionally, this study seeks to analyze the trajectory of seeds injected during the precipitation process and determine the optimal seed injection location for a more evenly distributed outcome. Based on the simulation results, the problem with the current precipitation process will be identified, and a form of the blade and seed inlet location that can increase mixing rates will be proposed.

2. Multi-phase CFD simulation

2.1. Govering Equation.

Computational fluid dynamic (CFD), which we know well, is mainly a single–phase flow that uses the Navier-stokes equation as a governing equation. Equation (2)

$$\rho g_x - \frac{\rho p}{\rho x} + \frac{\partial}{\partial x}\left(2\mu\frac{\partial u}{\partial x} - \frac{2}{3}\mu\nabla\cdot\vec{V}\right) + \frac{\partial}{\partial y}\left[\mu\left(\frac{\partial u}{\partial y} + \frac{\partial v}{\partial x}\right)\right] + \frac{\partial}{\partial z}\left[\mu\left(\frac{\partial w}{\partial x} + \frac{\partial u}{\partial z}\right)\right] = \rho\frac{\partial u}{\partial t} + \rho(\vec{V}\cdot\nabla)u \qquad (2)$$

However, $TiOSO_4$ Solution meets introducing gas type wet steam in the precipitation tank, and phase changing occurs. Results of multiphase flow, force, and mass exchanges also take place. Therefore, the following governing equation Equations (3) and (4) should be used for multi-phase flow.

$$\text{Continuity}: \frac{\partial(\alpha_q\rho_q)}{\partial t} + \nabla\cdot(\alpha_q\rho_q u_q) = \sum_{p=1}^{n}\dot{m}_{pq} \qquad (3)$$

$$\text{Energy}: \frac{\partial(\rho U)}{\partial t} - \frac{\partial\rho}{\partial t} + \nabla\cdot(\rho U h_{tot}) = \nabla\cdot(\kappa\nabla T) + \nabla\cdot(U\nabla\tau) + S_M \qquad (4)$$

The meaning of α_q is the Volume fraction of q^{th}phase, and the momentum equation of q^{th} phase can be written as the following Equation (5)

$$\frac{\partial(\alpha_q\rho_q u_q)}{\partial t} + \nabla\cdot(\alpha_q\rho_q u_q) = -\alpha_q\nabla p + \alpha_q\rho_q g + \nabla\cdot\tau_q + \sum_{p=1}^{n}(R_{pq} + \dot{m}_{pq}u_q) + \alpha_q\rho_q(F_q + F_{lift,q} + F_{vm,q}) \qquad (5)$$

Where $\boldsymbol{R_{pq}}$ is interphase forces exchange, and $\boldsymbol{\dot{m}_{pq}u_q}$is interphase mass exchange. Ansys CFX 18.2 is used for governing equations and multiphase solver. The turbulence modeling utilized in this study was the Detached Eddy Simulation (DES).

2.2. Geometry and mesh generation

The system design consists of three essential components: the primary tank, an agitator, and a steam nozzle. The primary tank has a diameter of 3.96 meters, while the agitator measures 1.44 meters in length. The steam nozzle is equipped with three injection holes. The arrangement of these components is illustrated in Figure 1

Preprints (www.preprints.org) | NOT PEER-REVIEWED | Posted: 13 September 2023 doi:10.20944/preprints202309.0877.v1

Figure 1. Tank, Agitator, Steam nozzle geometry.

The computational domain consists of two distinct zones: a rotating zone that includes the agitator and a fixed zone that does not contain the agitator. These two domains communicate with each other using the General Grid Interface (GGI). However, the rotation of the agitator leads to changes in the cell centers at the interface, which can decrease the accuracy of the calculations. To address this issue, a remeshing method is employed to adjust the cell centers at each time step, thereby improving the accuracy of the calculations.

In total, approximately 4 million unstructured grids are generated in the rotating zone, while 6 million unstructured grids are generated in the fixed zone. This results in a total of 10,348,194 elements and 4,885,988 nodes being constructed. The mesh generation and computational domain are depicted in Figure 2

In order to apply the Detached eddy simulation (DES) turbulence modeling, 10 layers are generated around the blade with a growth rate of 1.05. The value of Y+ (the nondimensional distance to the wall) is set to 1, ensuring that the turbulence model accurately captures the flow characteristics near the blade.

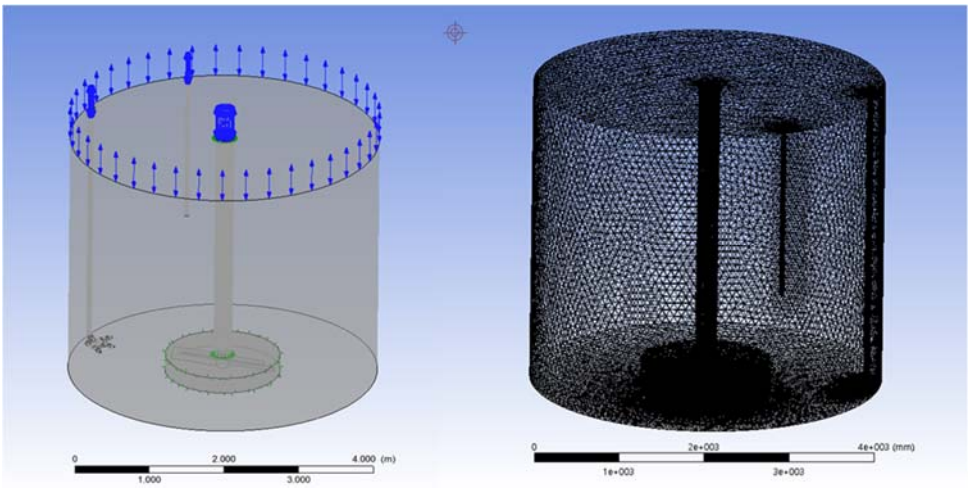

Preprints (www.preprints.org) | NOT PEER-REVIEWED | Posted: 13 September 2023 doi:10.20944/preprints202309.0877.v1

Figure 2. Computational domain and mesh generation

In this simulation, two different fluids are used. The first fluid is a solution of $TiOSO_4$, which is contained in the precipitation tank and maintained at a temperature of 55°C. The second fluid is wet steam, introduced from a steam nozzle, and has a temperature of 141°C. The properties of the $TiOSO_4$ solution, wet steam, and initial conditions can be found in Table 1 below. Additionally, for the purposes of this simulation, a solid-type seed is utilized. The detailed properties of the seed are proprietary information of the company and cannot be disclosed.

Table 1. Property of $\boldsymbol{TiOSO_4}$ and wet steam

Identification	$\boldsymbol{TiOSO_4}$	Wet steam
m (Molar mass)	159.92 g/mol	18.01528kg/kmol
ρ (Density)	1.5954 g/cm^3	1.96847 kg/m^3
c (Specific heat capacity)	1070 J/kg.K	1.9130kJ/kg.K
μ (Dynamic viscosity)	0.001kg/ms	0.00001kg/ms
κ (Thermal conductivity)	0.6W/m.K	0.003W/m.K
Initial condition	1atm 55℃	3.9bar 141℃

Tank wall and steam nozzle surface are set with no-slip wall boundary conditions. The open boundary condition has a zero volume fraction of $TiOSO_4$, allowing only steam to flow out through the free surface. To make the simulation as realistic as possible, steam with a turbulence intensity of 30% is injected. The seed inlet is located both at the side inlet and the central part, as shown in Figure 3, which describes the boundary conditions.

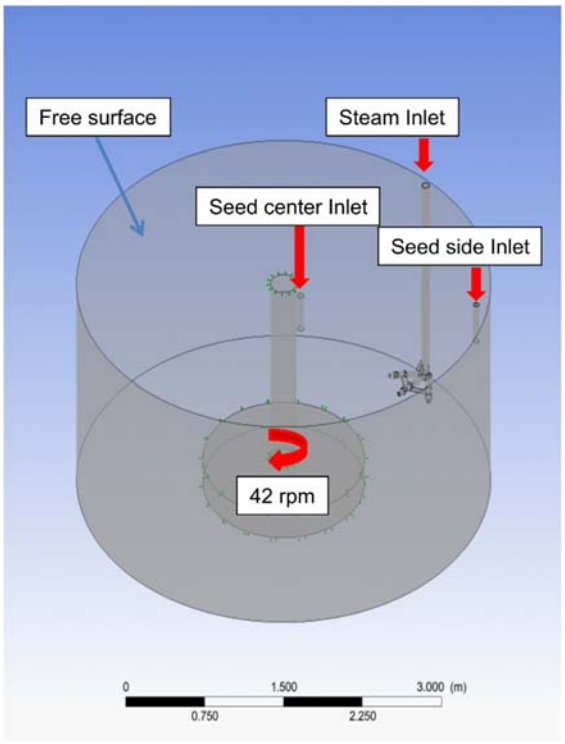

Figure 3. Boundary condition of computational domain

2.4. Numerical analysis of single-stage Agitator

A simulation was conducted by changing the position of the seed inlet for a 1440mm single-stage blade currently used in the field and a 1940mm blade, which had the highest mixing rate among single-stage blades [17]. To validate a developed 3-phase multiphase CFD code, a comparison and analysis was made between the average temperature on each plane and the temperature in the field. The code validation results are explained in Table. 2 blow

Preprints (www.preprints.org) | NOT PEER-REVIEWED | Posted: 13 September 2023 doi:10.20944/preprints202309.0877.v1

Table 2. Temperature comparison between CFD and Actual field (1440mm single)

Location	CFD (℃)	Actual field (℃)
Bottom	115.858	112.8
Middle	113.863	111.3
Top	101.241	97.9
Side	113.495	109.7
Average	112.682	108.1
Bottom	115.858	112.8

As shown in the left side of Figure 4 represents the volume fraction of steam discharged from the steam nozzle and right side of Figure 4 indicates the steam volume fraction from the agitator. Mass and heat transfer between steam and solution has occurred.

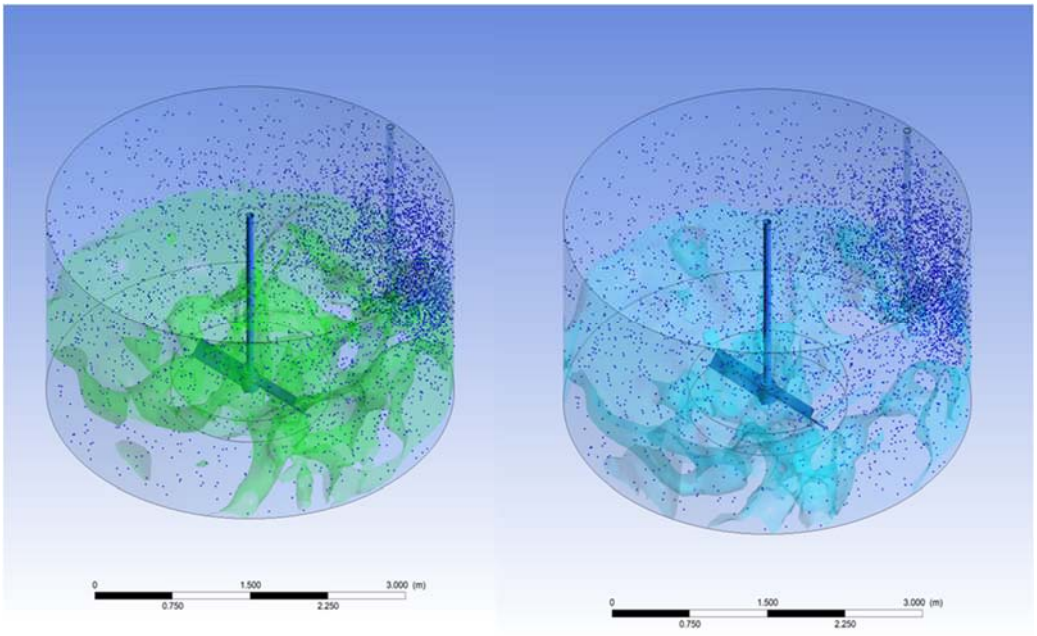

Figure 4. Particle distribution of seed in the precipitation tank

As can be seen in the Fig5. when the seed is input through the side inlet, a large amount of seed accumulates on the left side of the tank and cannot be dispersed.

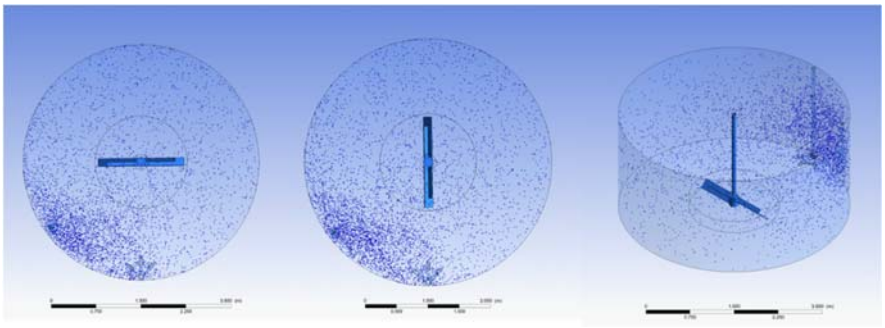

Figure 5. Top view of particle distribution

The process design consists of three essential components: the primary tank, an agitator, and a steam nozzle. The precipitation occurs most actively at the initial stage when the seed is added. Therefore, the early stage of seed addition is more critical than the state where the distribution is uniformly achieved after a sufficient time. Accordingly, this study analyzes the dispersion within 5 minutes after seed addition.

Preprints (www.preprints.org) | NOT PEER-REVIEWED | Posted: 13 September 2023 doi:10.20944/preprints202309.0877.v1

It is difficult to describe the agglomeration phenomenon of nano-sized particles using CFD, and it is almost impossible to represent of primary particles. Therefore, in this paper, it is assumed that uniform-sized agglomerates grow when the injected seed is evenly distributed. When the seeds are not evenly distributed, $\boldsymbol{TiO_2}$ particulates of less than 100nm are produced by heat and water, which we call pre-hydrolysis. To make a uniform particle size distribution, the optimized blade design is required to avoid pre-hydrolysis,

In the case of a side inlet, it was not possible to obtain uniform seed dispersion regardless of the location in a circular tank. Moreover, as shown in Figure 6, upon observation of the actual site, a significant amount of scale was found to form in the same location where seed had accumulated, on the left side of the nozzle as predicted by the CFD simulation.

Figure 6a illustrates the region around the nozzle in the currently operated precipitation tank, demonstrating that more scale is generated on the left wall of the tank compared to the right wall. Figure 6b provides an enlarged view of the left wall of the tank, further confirming the substantial scale formation in the area where the seed particles are not dispersed but rather accumulated, consistent with the CFD predictions.

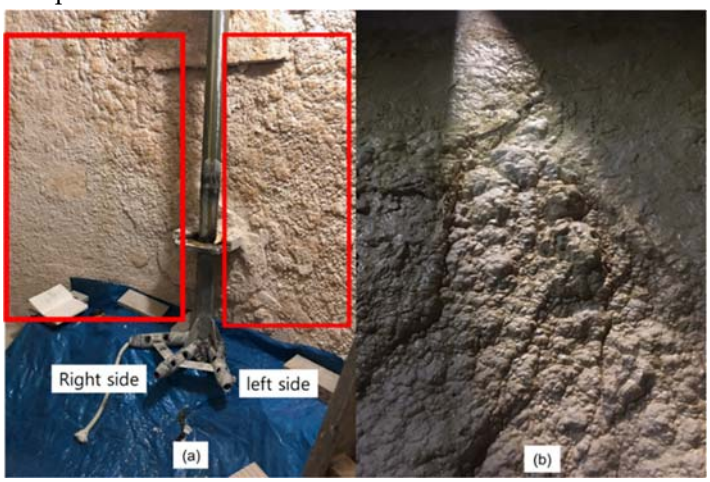

Figure 6. Wall scale formed by precipitation

To identify the seed distribution, the tank was divided into eight sections, and the density of particles in each area was measured, as shown in the following Figure 7 and results are presented in Figure 8

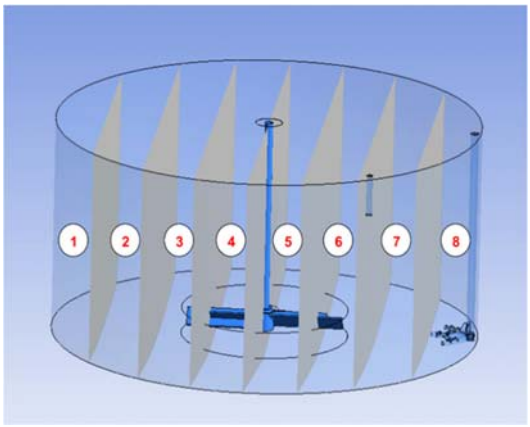

Figure 7. 8 regions of precipitation tank

Preprints (www.preprints.org) | NOT PEER-REVIEWED | Posted: 13 September 2023 doi:10.20944/preprints202309.0877.v1

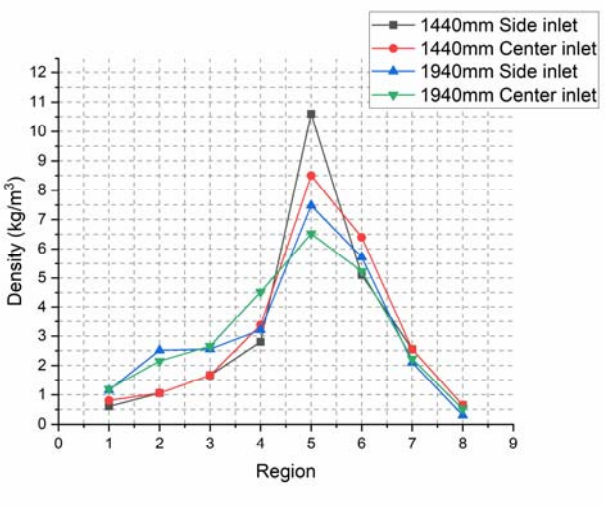

Figure 8. Seed distribution of each region (single blade agitator)

As can be seen from the Figure 8, for the side inlet, both the 1440mm and 1940mm single stage blades have the highest concentration of seeds in region 5, and the lowest distribution of seeds in zone 1. This is because the steam injected faster than the tip speed ratio reaches the wall and then rises along the wall. The risen seeds are rotated by the agitator and dispersed. Even upon inspecting the interior of the tank, it can be observed that a minimal amount of scale is generated on the wall of Region 1.

Additionally, the highest concentration of seeds in zone 5 can be attributed to the centrifugal force generated by the rotation of the agitator, which causes the seeds to spread towards both the central and wall areas of the tank. In terms of the relationship between mixing rate and dispersibility, it is evident that the seeds are more evenly dispersed with the more efficient mixing rate of the 1940mm single-stage blade. Figure 8 depicts the top view of different seed inlets for the 1440mm and 1940mm blades, respectively.

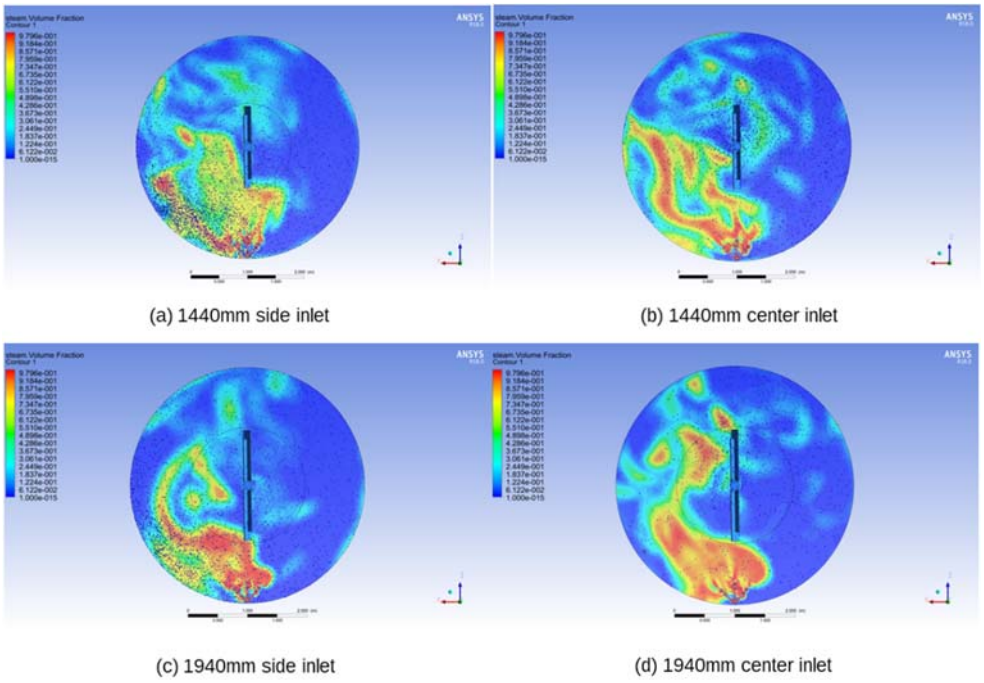

Figure 8. Seed distribution of different seed inlet

Preprints (www.preprints.org) | NOT PEER-REVIEWED | Posted: 13 September 2023 doi:10.20944/preprints202309.0877.v1

2.5. Numerical analysis of Double-stage Agitator

In Chapter 2.4, the performance of the single stage blade agitator was analyzed by changing the seed injection position. It was found that higher mixing efficiency and a more uniform distribution of the seed were achieved with a 1940mm blade compared to a 1440mm blade. Furthermore, the use of center inlet for seed injection resulted in a more uniform distribution than side inlet. The performance of a double stage blade agitator with a lower blade length of 1440mm and an upper blade length of 960mm, installed by a distance of 1400mm, was also analyzed.This optimized blade shape was explained by anothor paper[17]. For Comparing the mixing rate of $TiOSO_4$ solutoin, this study using Root Mean Square (RMS) values. The calculation of RMS is explained in Equation (6)

$$RMS = \frac{\sqrt{\frac{\int (T-\bar{T})^2}{A}}}{\bar{T}} \tag{6}$$

Where $\bar{T}$ represents the average temperature of the precipitation tank, and T represents the temperature in each cross-sectional area. Comparing the RMS values of a single blade agitator and a double blade agitator, the results are shown in the following Table 3.

Table 3. RMS of single and double blade agitator

Location	1440mm	1940mm	Double stage blade
Bottom	24.614	19.184	16.683
Middle	5.33	8.748	5.322
Top	14.163	13.498	11.893
Side	7.178	4.117	4.547
Average	12.821	11.387	9.611

As seen from the mixing rate depending on the blade type, the optimized double stage blade showed the highest mixing rate, and it is therefore considered to have the best seed distribution. This will be also confirmed by analyzing the seed distribution. The following Figure 9 shows the particle trajectory of the seed in the double stage blade, demonstrating that even with the side inlet, it has a more uniform particle distribution than the single stage blade. Moreover, using the center inlet results in an even more uniform particle distribution.

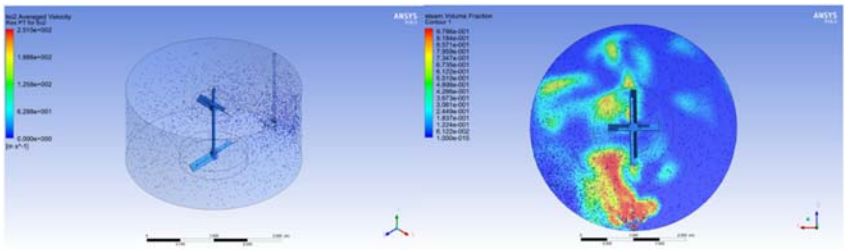

(a) Double stage - side inlet

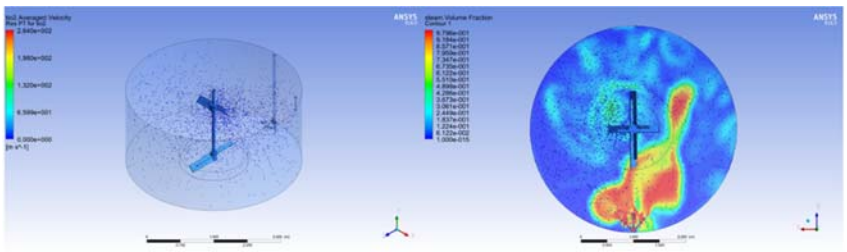

(b) Double stage - center inlet

Figure 1. Particle distribution of seed with double stage blade

Preprints (www.preprints.org) | NOT PEER-REVIEWED | Posted: 13 September 2023 doi:10.20944/preprints202309.0877.v1

For quantitative analysis, the tank was divided into eight regions as shown in Figure 7, and the seed density in each region was measured agin.

It is confirmed that there is no change in the total amount of seed, and the distribution of seed for each blade can be seen in the Table 4 and Figure 10.

Table 4. Comparison of seed distribution among different blade lengths in each region

	1440mm single blade		1940mm single blade		Double blade	
	Side inlet (kg/m^3)	Center inlet (kg/m^3)	Side inlet (kg/m^3)	Center inlet (kg/m^3)	Side inlet (kg/m^3)	Center inlet (kg/m^3)
Region 1	0.61	0.81	1.16	1.2	1.56	2.75
Region 2	1.06	1.06	2.52	2.15	2.07	2.35
Region 3	1.665	1.665	2.56	2.66	3.44	2.95
Region 4	2.8	3.374	3.21	4.52	4.08	4.9
Region 5	10.6	8.5	7.48	6.52	6.11	5.65
Region 6	5.1	6.4	5.72	5.23	4.28	4.25
Region 7	2.55	2.55	2.1	2.23	2.1	1.6
Region 8	0.65	0.65	0.31	0.52	1.42	0.61
Total Seed	71.97kg	71.88kg	71.84kg	71.96kg	72.04kg	71.94kg

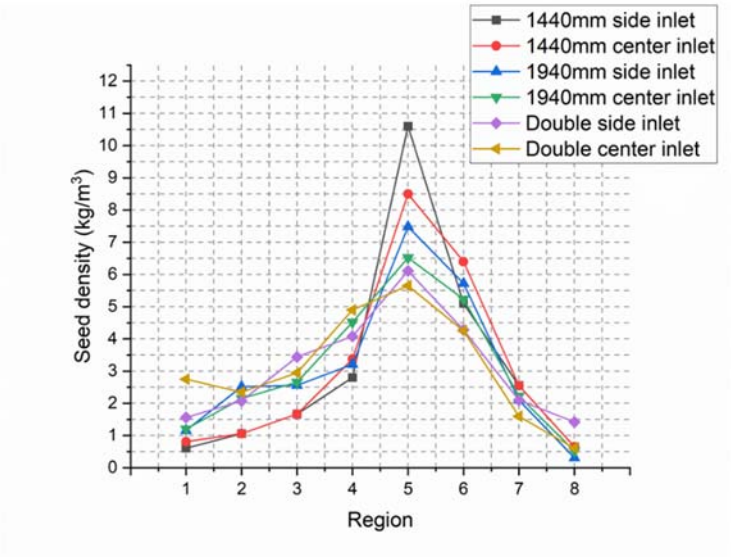

Figure 10. Particle distribution of seed with single and double stage agitator

As can be seen in the above Figure 10, there is a slight difference between the center inlet and side inlet configurations in the optimized double blade with a high mixing rate. By slightly shifting the distribution of seed towards region 1 through the center inlet, a more uniform precipitation process can be achieved.

3. Lab scale experimental results

Preprints (www.preprints.org) | NOT PEER-REVIEWED | Posted: 13 September 2023 doi:10.20944/preprints202309.0877.v1

The double-blade agitator, confirmed through CFD analysis, exhibits a superior solution mixing rate compared to the single-blade agitator currently in use. To validate chemical reactions during the seeding process, it is imperative to carry out laboratory-scale experiments and real-world field tests. To begin with, a scaled-down model experiment was conducted using an actual precipitation tank system at a ratio of 1:32.8, with the dimensions of the reduced model detailed in Table 5.

Firstly, a reduced model experiment was conducted on an actual precipitation tank system of 1:32.8, and the dimensions of the reduced model are shown in Table 5.

Table 5. Reduced model dimension

	Actual	Reduced model
Tank external diameter	3940mm	120mm
Amount of solution	23000m^3	700m^3
Lower blade	1440mm	43.8mm
Upper blade	960mm	29.2mm
Distance between two blades	1400mm	42.6mm
Agitator column diameter	165mm	5mm
Tank bottom to blade length	300mm	9mm

In Figure 11 below, the explanation includes: a) the 1440mm scale reduction model, b) the 1960mm scale reduction model, and c) the double-stage blade scale reduction model. These three primary blade variations underwent testing to assess the agitator's performance. The precipitation experiment setup is illustrated in Figure 12, with a detailed test procedure outlined in Table 6 further below. The tests were conducted within a glass reactor. In the real-world application, steam is employed to raise the temperature. However, due to constraints in laboratory-scale experiments, which involve challenges in steam generation and maintaining a steady supply, the temperature was elevated using a heating mantle and water at 100°C. Additionally, a condenser linked to a coolant system was installed to prevent concentration effects arising from evaporation.

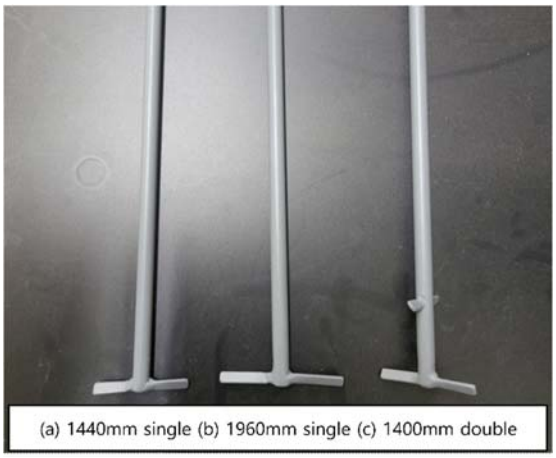

Figure 11. single and double blade for experiments

The temperature control system was set up for automatic operation with a predefined interval. This automated temperature control system connects a temperature sensor and a Temperature Controller to the heating mantle. The concentration of titanium (Ti) and the quenching process in the $\boldsymbol{TiOSO_4}$ solution, used for single decomposition, typically ranges from 180g/L to 220g/L and is considered proprietary technology. Therefore, a specific quantity of water at 95°C is added to a beaker for stable test. This water is heated using a heating mantle, and any evaporated water is condensed and returned through a condenser and chiller. The precipitation process comprises several

Preprints (www.preprints.org) | NOT PEER-REVIEWED | Posted: 13 September 2023 doi:10.20944/preprints202309.0877.v1

stages, including initial heating, seed injection, aging, secondary heating, and temperature stabilization. Seed injection occurs when the solution temperature reaches 96°C. The crucial aspect of seed injection is ensuring the uniform dispersion of the seed into the tank. To maintain similarity with the process, the rotational speed of the agitator is a critical factor in these laboratory experiments.

Once the precipitation process is completed, the mother liquor is subjected to filtration using a 5-micron filter until the residual iron content reaches a level of 100 mg/L. After the initial washing, water is poured onto the resulting cake, and re-pulping is carried out. The resulting solution is then mixed with sulfuric acid and aluminum powder and heated to 70°C for bleaching. This bleaching process effectively removes chromium, arsenic, and iron. Subsequently, a second washing is performed using the same method as the first washing until the residual iron content reaches 3 mg/L. The resulting $\boldsymbol{TiO_2}$ solid is subjected to calcination in an electric furnace. The temperature is gradually increased from 350°C to 950°C over two hours and maintained at 950°C for one hour. Following calcination, the $\boldsymbol{TiO_2}$ solid is pulverized using a pulverizer equipped with a 0.2 mm mesh. Analytical equipment such as ICP-OES, ICP-MS, XRF, and Microtrac is employed to assess heavy metal content, particle size, and distribution.

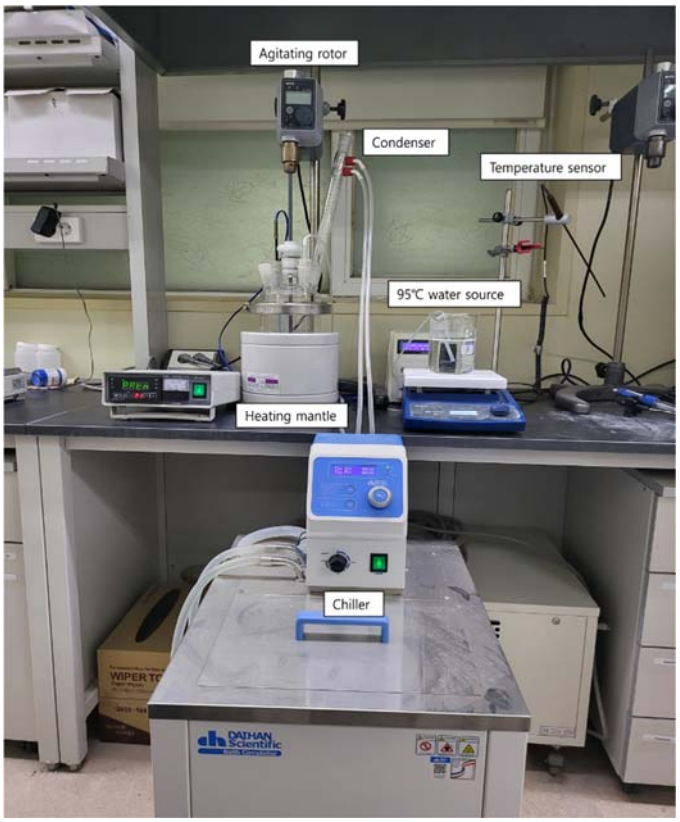

Figure 12. Experimental apparatus

Table 6. Lab test procedure

#	Procedure	Remark
1	First heating (80℃→110℃)	60min
2	Seed introducing at 94℃	5min
3	Aging (no heating)	30min
4	Second heating (90℃ → 110℃)	30min
5	Constant Temperature	180min
6	First washing with 5c filter	Fe 100mg/L ↓
7	Repulping	

Preprints (www.preprints.org) | NOT PEER-REVIEWED | Posted: 13 September 2023 doi:10.20944/preprints202309.0877.v1

8	Bleaching (70℃)	Al powerder + H_2SO_4
9	Second wahing with 5c filter	Fe: 3mg/L ↓
10	Dehydrate	Humidity 50% ↓
11	Calcination 350℃ → 950℃	120min
12	Calcination 950℃	60min
13	Miling	Pulverizer 3times with 0.2mm mesh

To ensure experimental similarity, selecting the Reynolds number would lead to a high RPM that exceeds testing capabilities. Consequently, we opted for the lab experiment to utilize the Froude number Equation (7), which accounts for inertia and gravity.

$$\boldsymbol{Fr = \frac{V}{\sqrt{gL}}} \tag{7}$$

Where Fr is the Froude number, V is the velocity of the agitator blade (m/s), g is the acceleration due to gravity (m/s²), and L is the diameter of the impeller (m). The rpm, which is related to the Froude number, was adjusted through checalc.com which is web application that calculates various physical properties used in chemical experiments. This web application can perform scale-up and scale-down based on criteria such as equal tip speed, power per unit volume, equal Reynolds number, Froude number, etc., using real field data. Results are described in Table 7.

Table 7. Dimensions for experimental similarity

Contents	Units	Lab scale	Actual field
Volume	m^3	0.001	23
Vessel diameter	mm	120	3940.2
Liquid level	mm	57.5	1887.5
Equivalent diameter	mm	93.9	3083
Shaft speed	rpm	240	42
Froude number		$7.83e^{-2}$	$7.83e^{-2}$
Reynolds number		14746	2774368
Tip Speed	m/s	0.6	3.46

Throughout the heating process, bubbles naturally formed in both the actual field and laboratory experiments. In the actual field, these bubbles typically had a negligible size. However, in the lab tests, these bubbles had a significant impact on the mixing rate. To mitigate this effect, the initial heating was carried out with minimal heat for an extended period before seed injection. However, during the second heating stage, which required a temperature of 110°C, it was challenging to avoid bubble formation in the lab-scale experiment. Additionally, due to the influence of these bubbles, it was difficult to discern the differences between the side inlet and center inlet methods of seed injection in the experiments.

Nonetheless, as illustrated in Figure 13 below, the particle distribution in experiments utilizing a double-stage blade configuration was superior to that of a single-stage blade. Each test was conducted three times, and the average data from these test results were compared. Figure 14 provides an explanation of the Transmission Electron Microscopy(TEM) analysis.

Preprints (www.preprints.org) | NOT PEER-REVIEWED | Posted: 13 September 2023 doi:10.20944/preprints202309.0877.v1

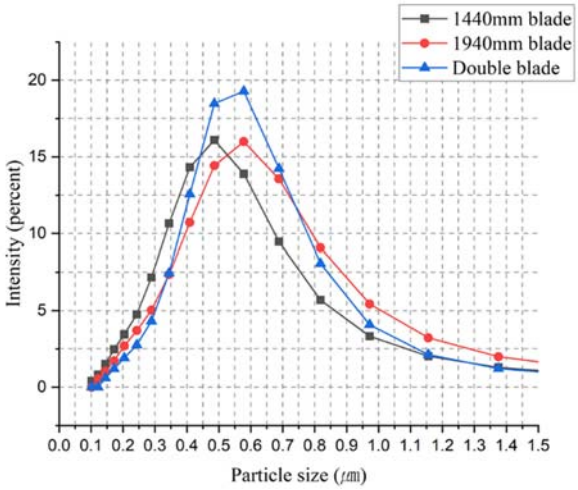

Figure 13. Particle distribution of single and double blade.

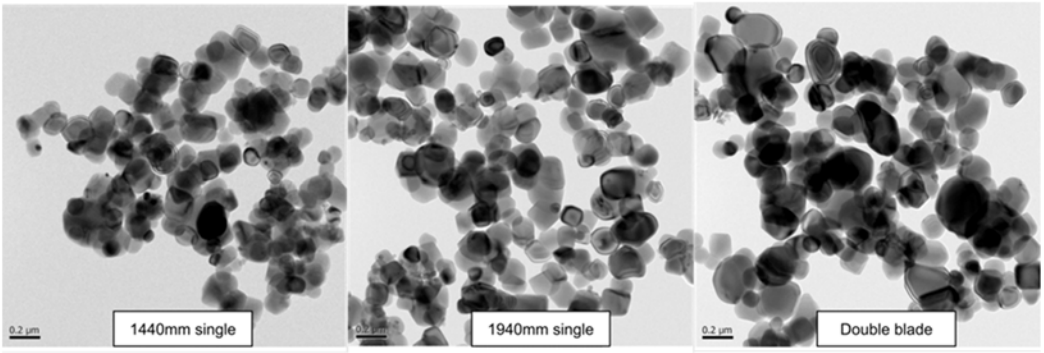

Figure 14. TEM analysis of particle distribution

4. Actual field test results

For the Actual field test, one of the precipitation tanks in operation was set double-stage blade verified with CFD and a lab-scale test. The single and double-stage blades are explained in Figure 15. Take the liquid samples from two different types of precipitation tanks and analyze particle distribution. The particle distribution is explained in Figure 16. Malvern planetary was used to analyze particle size distribution

Figure 15. Single (1440mm) and Double stage blade installation in precipitation tank

Preprints (www.preprints.org) | NOT PEER-REVIEWED | Posted: 13 September 2023 doi:10.20944/preprints202309.0877.v1

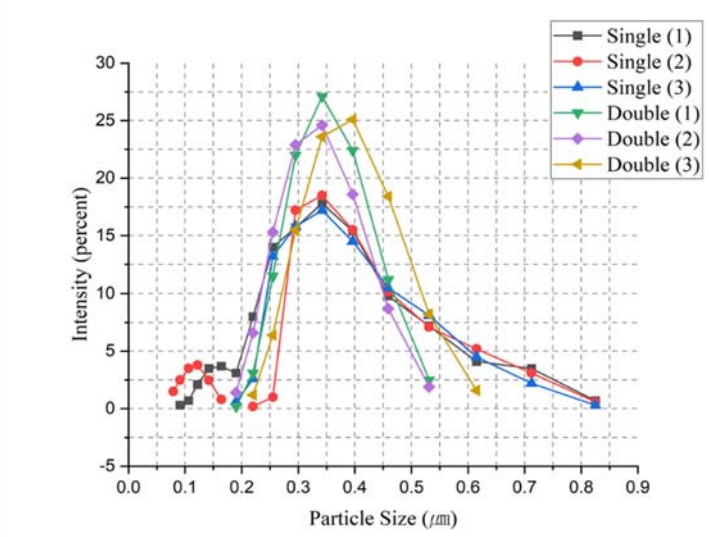

Figure 16. Particle distribution by intensity

Figure 17 is a TEM photograph of the particle distribution. Several fine particles less than 100nm were counted in single-blade cases, and the uniformity of particle size distribution was increased compared to a single-blade.

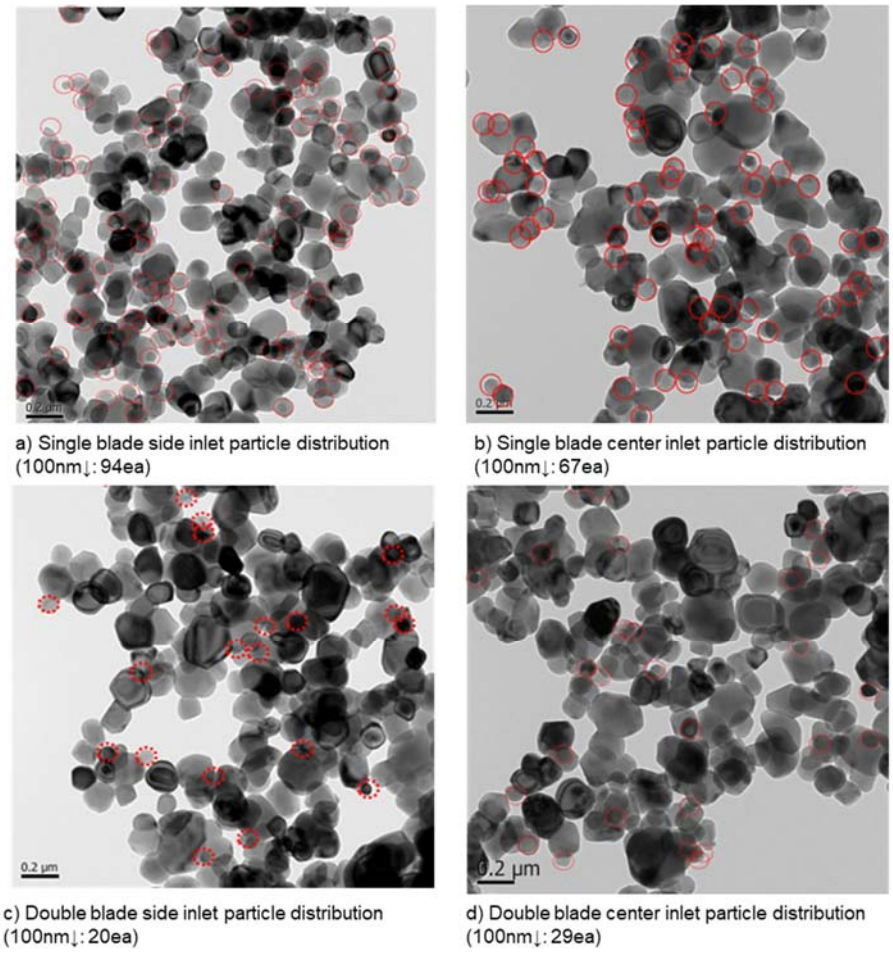

Figure 17. Tem analysis of single and double stage blade with different seed inlet

In this study, a settling value test, widely employed for assessing particle size uniformity, was conducted. Subsequently, we aim to perform a comparative analysis of particle distribution between

Preprints (www.preprints.org) | NOT PEER-REVIEWED | Posted: 13 September 2023 doi:10.20944/preprints202309.0877.v1

the single blade and double blade configurations. The settling value test involves diluting 114ml (190g/L TiO_2) of the hydrolyzed solution with 300ml of water. After cooling to 25 degrees, additional water is added to make up a 500ml solution. After 30 minutes, the suspension length is measured. A high settling value indicates a broader accumulation of smaller particles in the gaps between larger particles, resulting in a longer suspension length. On the contrary, a low settling value demonstrates that larger than 400nm TiO_2 particles are uniformly generated and there are significant presence of voids between particles.

This study determined that the optimal washing efficiency of the Moore Filter (MF) used in the Cosmo chemical process was 50 mm/30 min. It was found that the 1440 mm single-blade and side inlet, which had the lowest mixing rate in this study, had a settling value of over 67. The increase in settling value indicates that the development of flocs between particles is high and that there is a significant difference in particle size. The following Figure18 and Table 8 represent the results of the settling value test for single blade and double blades with center seed inlet.

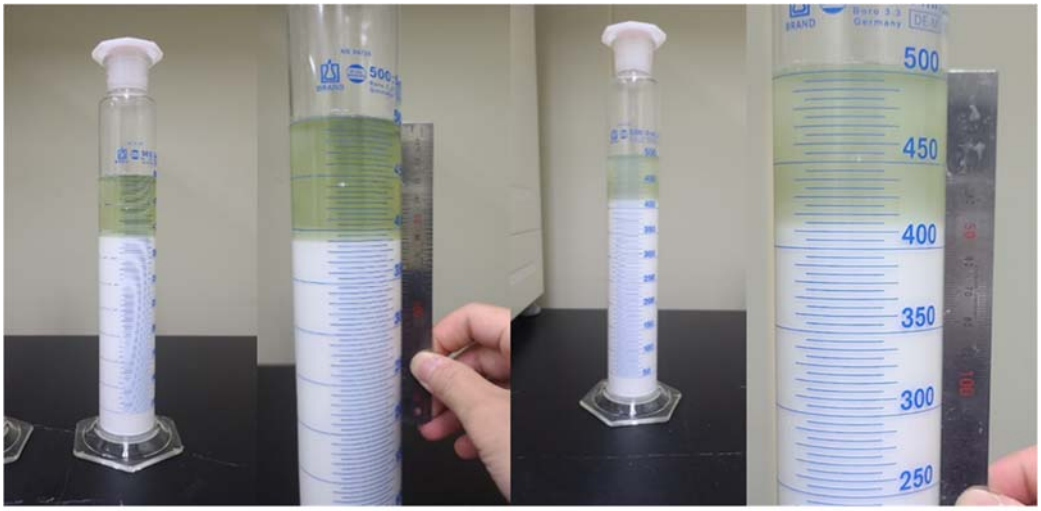

Figure 18. Settling value test for single and double blades

Table 8. Settling value of different blade types

Blade type	Settling value Case1	Settling value Case2	Settling value Case3
1440mm single blade	63	60	61
Double stage blade	51	48	49

5. Results

This study primarily focuses on optimizing the operational parameters of the precipitation process through Multiphase CFD simulation, lab scale experimental and actual field tests, with the main goal of achieving a uniform particle size distribution. A Fluid-Gas-Solid coupled multiphase solver, explicitly tailored for handling precipitation involving solid-type seeds, was developed. This 3-phase CFD solver enables the identification of the distribution and trajectory of seeds that cannot be visually observed, establishing a strong correlation between the mixing rate and seed distribution.

As the mixing rate of the $TiOSO_4$ solution and steam increased, a more uniform distribution of seeds was achieved, effectively minimizing pre-hydrolysis in areas devoid of seeds. Consequently, the utilization of a double-stage agitator with a high mixing rate resulted in a notable decrease in the number of particles below 100 nm, accompanied by a pronounced centralization of the particle distribution. Moreover, it was observed that using a center inlet for seed injection in a single-stage blade yielded a more uniform seed distribution compared to a side inlet.

 doi:10.20944/preprints202309.0877.v1

In the context of a double blade, which boasts a high mixing rate, both side inlet and center inlet configurations produced uniform seed distributions. However, using a center inlet demonstrated superior performance by ensuring an even particle distribution through the uniform supply of seeds to the opposite side of the nozzle. This uniform particle distribution not only facilitated consistent precipitation but also hindered the formation of particles smaller than 100 nm.

In conclusion, the optimized blade, as validated by CFD, demonstrated exceptional mixing capabilities during field experiments within the precipitation process. It not only ensured a uniform temperature distribution of $TiOSO_4$ solution but also created a consistent seed distribution. Additionally, by operating the precipitation process uniformly and stably, TiO_2 particles with a uniform size could be produced. This enhanced uniformity in TiO_2 distribution played a pivotal role in improving settling value and filtration seconds. The optimization of the precipitation process, as the key outcome of this research, had a significantly positive impact on the subsequent washing process. This resulted in a substantial improvement in productivity efficiency and played a pivotal role in the high-quality production process of TiO_2.

Acknowledgement: This research was supported by COSMO Chemical Co., Ltd.

References

1. Kristen, G.; lvana, F.; Emanuele, C.; Julia, K. Distinctive Toxicity of Rutile/Anatase mixed phase nanoparticles, Chem. RES.Toxicol. 2012, 25, 646-655
2. Braun,J.H.; Baidins,A.; Marganski, R.E. A Review of the production cycle of Titanium dioxide pigment, A review. Prog. in org. coating, 1992, 20, 105-138,
3. Kang J.S,; Toru H.O. Production of Titanium Dioxide Directly from Titanium Ore through selective Chlorination using Titanium Tetrachlorie. Mater.Trans, 2014, 55, 591- 598
4. Laware S.L.; Shipha, R.; Effect of Titanium Dioxide Nanoparticles on Hydrolytic and Antioxidant Enzymes druring Seed Germination in Onion, Int. J. Curr. microbio. 2014, 3, 749-760
5. Egor, A.; Moskalenko, A.A.; Sadovnikov, A.E. Synthesis of Nanocrystalline Titania via Microwave-Assisted Homogeneous Hydrolysis under Hydrothermal Conditions, Curr. Microw. Chem., 2014, 1, 81–86
6. Albena, B.N.; Stancho, Y.; Reni, I.; Irina, S. The Solvent Role on the Hydrolysis-Condensation Process and Obtaining of TiO2Nanopowders, J. Chem. Technol. Metall., 2018, 54, 292–302
7. Min, Z.; Naofumi, U.; Takashi, K.; Kazuyuki, K. Characterization of TiO2 Photocatalyst Nanoparticles Prepared by Low Temperature Hydrolysis Reaction of Alkoxides, Proc. Int. Eco. Sci., 2007, 1, 788–790
8. Andreas, L.; Thomas, S.; Permorsing, L. Urea decomposition and HNCO hydrolysis studied over titanium dioxide, Appl. Catal., B, 2011, 106, 273-279
9. Windler L.; Lorenz. C; Nvon, G.; Hungerbuhler, K. Release of Titanium Dioxide from Textiles during washing, Environ. Sci. Technol. 2012. 46, 8181-8188
10. Zouhir, E.; Allouni, H.; Mihaela, R.; Cimpan, P.; Hol, J. Agglomeration and sedimentation of TiO2 nanoparticles in cell culture medium, Colloids Surf., B. 2009. 68, 83-87
11. Allisonk M.H.; Andrea C.N.; Randall, E; Mielke, H, Dispersion of TiO2 Nanoparticle Agglomerates by pseudomonas aeruginosa, Appl. Environ. Microbiol. 2010, 76, 7292-7298
12. Plazl. I; Leskovsek. S; Koloini, A. Hydrolysis of sucrose by conventional and microwave heating in stirred tank reactor, Chem.Eng.J. 1995, 59, 253-257
13. Barbara, G.; Daniel, G.; Bogumil, K. Effects of Processing Parameters on Hydrolysis of TiOSO4, J. Chem. Technol., 2009, 11, 15–21
14. Kim, K.D.; Lee, T.J.; Kim, H.T. Optimal Conditions for Synthesis of TiO2 Nano Particles in SemiBatch Reactor, Colloids Surf. A Physicochem. Eng. Asp., 2003, 224, 1–9
15. Thong, L.B; Gyula, G.; Vincent, O.O. A CFD Study on Heat Transfer Performance of SiO2-TiO2 Nanofluids under Turbulent Flow, J. Nanomater, 2022, 12, 299–302
16. Kaya. H; Ekiciler. E.; Arslan. B. CFD Analysis of laminar forced convective heat transfer for TiO2/water nanofluid in semi-circular cross-section micro- channel, J. Ther. Eng. 2019, 5, 123-137
17. Han, J.H.; Hyojong, K.; Dohyoung, L. Parametric study of agitator in TiO2 precipitation tank using multiphase CFD simulation and experiments, J. Enhanced heat transfer,2023, 30, 1-20